

Accepted May 3rd 2022**Magneto-convective flow through a porous enclosure with Hall current and Thermal radiation effects: Numerical study*****K. Venkatadri¹*, O. Anwar Bég² and S. Kuharat²****¹Department of Mathematics, Siddhartha Institute of Science and Technology, Puttur-517581, A.P., India.**²Multi-Physical Engineering Sciences Group, Aeronautical/Mechanical Engineering, Salford University, School of Science, Engineering and Environment (SEE), Manchester, M54WT, UK***Corresponding author- email: venkatadri.venki@gmail.com***Abstract**

This paper reports the numerical study of magnetohydrodynamic radiative-convective flow in a square cavity containing a porous medium with Hall currents. This study is relevant to hydromagnetic fuel cell design and thermofluidic dynamics of complex magnetic liquid fabrication in enclosures. The governing equations of this fluid system are solved by a finite-difference vorticity stream function approach executed in MATLAB software. A detailed parametric investigation of the impact of Rayleigh number (thermal buoyancy parameter), Hartman number (magnetic body force parameter), Darcy number (permeability parameter), Hall parameter and radiation parameter on the streamline, temperature contours, local Nusselt number along the hot wall and mid-section velocity profiles is computed. Validation with previous special cases in the literature is included. Hall current and radiative effects are found to significantly modify thermofluidic characteristics. From the numerical results, it is found that the magnetic field suppresses the natural convection only for small buoyancy ratios. But, for larger buoyancy ratio, the magnetic field is effective in suppressing the thermal convective flow.

Key words: *Magnetohydrodynamics; Enclosure; Finite difference Method; Hall current; Natural convection; Heat Transfer; Nusselt number; hybrid fuel cells; thermal buoyancy; thermal radiative flux.*

Nomenclature

B_0	Transverse magnetic field strength (Tesla)
C_p	Specific heat at constant pressure, $J\ kg^{-1}\ K^{-1}$
Da	Darcy number

Ha	Hartmann (magnetic body force) number
h	Convective heat transfer coefficient, $\text{Wm}^{-2} \text{K}^{-1}$
k	Thermal conductivity of the magnetic viscous fluid, $\text{Wm}^{-1} \text{K}^{-1}$
K	Permeability (m^2)
L	Length of walls, m
m	Hall current parameter
Pr	Prandtl number
Ra	Rayleigh number
Rd	Thermal radiation parameter
g	Acceleration due to gravity (m/s^2)
Nu	Local Nusselt number
T	Temperature ($^{\circ}\text{C}$)
(u, v)	Cartesian velocity components (m/s)
(U, V)	Dimensionless velocity components
(x, y)	Cartesian co-ordinates (m)
(X, Y)	Dimensionless co-ordinates
P	Pressure (pa)
T_c	Cold right wall temperature, $^{\circ}\text{C}$
T_h	Hot left wall temperature, $^{\circ}\text{C}$
t	dimensional time (s)

Greek Symbols

β	Thermal expansion coefficient, K^{-1}
β_r	Mean absorption coefficient
θ	non-dimensional temperature
σ^*	Electrical conductivity of viscous magnetic fluid, Siemens/m
σ	Stefan-Boltzmann radiation constant ($5.67 \times 10^{-8} \text{Wm}^{-2}\text{K}^{-4}$)
μ	Dynamic viscosity of the fluid, Nsm^{-2}
ρ	Density of the magnetic fluid, kgm^{-3}
α	Thermal diffusivity, m^2/s
ψ	Stream function
Ψ	Dimensionless stream function

1. INTRODUCTION

Magnetohydrodynamics (MHD) flow with heat transfer is one of the classes of flow in fluid mechanics which has received considerable attention in recent decades. This is due to the advancement of numerous transport processes in engineering and industries. Many new fluent media have been explored which respond to external electrical and magnetic fields [1] including ferrofluids, magnetic nanofluids, electro-conductive polymers, electrically conducting viscous fluids, magneto-rheological fluids etc [2]. Thermal convection heat transfer inside enclosures frequently features in fuel cell systems and also materials fabrication technologies. This is a complex branch of thermofluid dynamics and has been lucidly described by Gebhart et al. [3]. Thermal transport in enclosures is also relevant to Czochralski crystal growth technologies [5] and semiconductor synthesis [6].

Nevertheless, nowadays applications of magnetohydrodynamics are preferred with the strong applied magnetic field so that the impact of magnetohydrodynamics is perceptible. To simulate electromagnetic flows in enclosures both viscous magnetohydrodynamics (MHD) must also be considered in conjunction with thermal convection. Other thermophysical and hydrodynamic phenomena may also arise including Marangoni (surface tension), entropy generation [7] and species diffusion (mass transfer) [8]. The boundary value problems arising in enclosures (cavities) are generally strongly nonlinear and require robust computational approaches to simulate momentum and heat transfer characteristics. Many excellent investigations in magnetohydrodynamic enclosure convection flows have been reported in recent years, building on the classical studies reported in Gebhart et al. [3]. Mondal et al. [9] performed a control volume numerical technique to analyze the influence of partial wall motion on magnetohydrodynamic (MHD) convection induced by external forces in the cavity filled with a non-Darcy porous medium, with a corner heating arrangement and moving adjacent sides. They computed the streamlines, heatlines, temperature contours and average Nusselt number for various Richardson number, Reynolds number, Hartmann magnetic number, Darcy number and also porosities, observing that all these parameters and the partial wall motion significantly modify thermal characteristics in the enclosure. Haq et al. [10] deployed a finite element code to simulate the natural convection MHD flow in a cavity with wavy walls under a uniform transverse magnetic intense, with visualizations of streamlines and isotherms for a wide range of wavelength numbers, Rayleigh numbers and Hartmann numbers. They observed that with increment in Rayleigh number and wavelength parameter the heat transfer rate is boosted whereas the internal circulation is damped i.e., vortex cells are contracted with greater values

of Hartmann number (stronger intensity of magnetic field). Keyafati [11] used a hybrid finite difference Lattice Boltzmann method (FDLBM) to compute the laminar mixed convection of pseudoplastic water-alumina nanofluids in a two sided lid-driven enclosure under horizontal magnetic field, observing that greater Richardson number and Hartmann number both suppress heat transfer, whereas greater nanoparticle volume fraction elevates heat transfer.

The above studies neglected radiation heat transfer. Many fuels cell [12] and materials processing systems [13] however feature high temperature regimes. This invokes thermal radiative flux effects which can substantially alter the thermofluid characteristics. The optical thickness of the fluent media (e.g. working fluids in fuel cells, semiconductor melts etc) also has a dramatic influence on the efficacy of radiative transport in enclosures. Both gray and non-gray fluids may also arise. Several researchers have therefore considered coupled thermal convective-radiative transport in enclosure geometries. Since the general radiative heat transfer equation is very challenging to solve even numerically and complexity is further increased with simultaneous convection heat transfer, a popular approach in computational fluid dynamic simulation is to use a flux model [14] for addressing radiative flux effects. As noted earlier, magnetic convection flows are becoming increasingly important in materials technologies and hybrid fuel cell designs. The studies described earlier have however neglected the influence of Hall current effects. When electric current flows through a metal strip, electrons move laterally from one side of the material to the other. In the vicinity of an external magnetic field, the Lorentz magnetic force is generated which acts on the electrons. This causes a deviation in the path of the electrons, and results in a greater concentration of electrons on one side than on the other. A voltage is generated which is perpendicular to the direction in which the current flows. This is the classic Hall effect and induces a secondary flow in magnetohydrodynamics also known as cross flow. Hall current may exert a significant role in modifying transport characteristics in fuel cell design and materials synthesis in enclosure systems. Many studies have considered Hall current effect in viscous multi-physical MHD transport problems. Muiznieks et al. [15] (on thermomagnetic convection in polymer melts) and Saidin et al. [16] (on Hall mobility and conductivity in $Zn_xCd_{1-x}S$ mixed crystals). All these studies have confirmed that Hall currents exert a substantial role in viscous MHD flows and recommend the inclusion of this effect in more robust models. It is further noteworthy that Hall currents also arise in many other diverse applications including magneto-gas dynamics of spacecraft [17], ionized argon fuel cell systems [18], current sensors in electromagnetic measurements [19] and also Hall MHD generators in propulsion and energy systems [20]. Several studies have

examined Hall currents in enclosure MHD convection flows. Zhang et al. [21] used a finite volume method (FVM) and the Chandrasekhar discrete ordinates method (DOM) to analyze numerically Ohmic dissipation impact on magneto-convection in a radiatively participating fluid under the Hall effect in a square cavity with isothermal vertical walls and adiabatic horizontal walls. The analysis included absorption, emission, and scattering of the fluid and the reflection, absorption, and emission of the walls. They observed that Hall current and Joule heating strongly influences the streamlines, isotherms, Nusselt number, and the average temperature of the fluid. Zhang et al. [22] further investigated computationally the Hall effects on natural convection MHD flow in a gray fluid-filled square enclosure with thermal radiation. They considered an external uniform magnetic field and solved the general radiative transfer equation (RTE). They simulated in detail the temperature and velocity distribution modification with Hall current and observed that over a certain range of radiative flux, Hall effect and Hartmann number (magnetic body force parameter) exert a considerable impact.

The above studies on MHD convection in enclosures generally neglected the inclusion of porous media. Although porous media enclosure flows have been studied previously in the presence of magnetohydrodynamic effects [23-25]. Sankar et al. [30] presented detailed analysis on impacts of various key parameters on flow and thermal behaviour of three different **nanofluids** in the annular geometry having finite thickness at the inner cylinder. Sankar et al. [31] presented detailed analysis on Natural convection of a low Prandtl number electrically conducting fluid ($Pr = 0.054$) under the influence of either axial or radial magnetic field in a vertical cylindrical annulus. Venkatachalappa et al. [32] investigated the effect of axial or radial magnetic field on the double-diffusive natural convection in a vertical cylindrical annular cavity. Sivasankaran et al. [33] investigated the effect of discrete heating on free convection heat transfer in a rectangular porous enclosure containing a heat-generating substance. Girish et al. [34] investigated the laminar natural convection in the vertical double-passage porous annuli formed by three vertical concentric cylinders of which the middle cylinder is a thin and perfectly conductive known as baffle. Girish et al. [34] studied the fully developed mixed convection in open-ended annuli with viscous dissipation. The behaviour of ionized fluids under the effect of the magnetic field has entirely different traits in comparison to the non-ionized fluids. The ionized fluids are influenced by three major factors named (a) the magnetic force owing to an applied magnetic field, (b) the Hall force, because of electrons' collision, (c) the Ion slip force, owing to ions' collision. Most of the existing works state the flows influenced by the Lorentz force.

However, no attempt has been performed to study the transport of magneto- convection in a square porous enclosure in the presence of Hall current. The porous medium is simulated using a Darcian model valid for viscous-dominated low Reynolds numbers. Additionally, radiative heat transfer is included via the Rosseland diffusion approximation. A comprehensive mathematical model is therefore described for two-dimensional steady viscous magnetohydrodynamic radiative-convective flow in a square enclosure containing a Darcian porous medium with Hall currents. The formulated nonlinear boundary value problem comprising the mass, momentum and energy conservation equations with appropriate wall boundary conditions, is rendered dimensionless via appropriate scaling transformations. The resulting non-dimensional computational problem is solved numerically with a finite-difference vorticity stream function approach executed in MATLAB software. A complete parametric investigation of the impact of Rayleigh number, Hartman number, Darcy number, radiative parameter and Hall parameter on the flow and temperature fields is conducted.

2. GOVERNING EQUATIONS

The regime under study comprises unsteady laminar natural convection fluid flow and heat transfer in an electrically conducting viscous fluid within a square enclosure (of dimensions L by L) containing a Darcian porous medium, under a transverse uniform magnetic field. A schematic diagram of the domain of interest in an (x,y) coordinate system with boundaries is depicted in **Fig. 1**. Different thermal boundary conditions are imposed. The left wall is sustained at temperature T_H (hot wall), the right vertical wall at T_L (cold wall) and the upper and base walls are adiabatic. It is assumed that the fluid flow within the enclosure is in thermal equilibrium and the working fluid is incompressible. The thermophysical properties of the working fluid are considered to be constant except the density in the buoyancy term, which obeys the Boussinesq approximation. Constant isotropic permeability is assumed, and Darcy's law is implemented which is valid for low Reynolds number (viscous dominated) flows i.e., inertial porous medium effects are neglected. Chemical reaction, viscous dissipation, thermal dispersion, thermal stratification and Joule heating (Ohmic dissipation) effects are also ignored. Hall current is however present which generates a cross flow perpendicular to the imposed magnetic field. Based on these assumptions the governing equations i.e., the balance of mass, conservative of momentum and energy (heat) under the Boussinesq approximation can be expressed as follows.

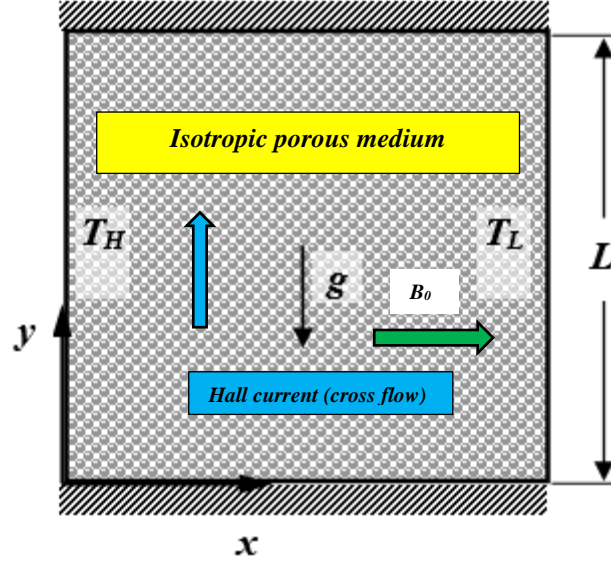


Fig. 1. Geometry of the magneto-convective enclosure flow problem

$$\frac{\partial u}{\partial x} + \frac{\partial v}{\partial y} = 0 \quad (1)$$

$$\rho \left(\frac{\partial u}{\partial t} + u \frac{\partial u}{\partial x} + v \frac{\partial u}{\partial y} \right) = -\frac{\partial p}{\partial x} + \mu \left(\frac{\partial^2 u}{\partial x^2} + \frac{\partial^2 u}{\partial y^2} \right) - \frac{\mu}{K} u - \frac{\sigma^* B_0^2}{1+m^2} (u - mv) \quad (2)$$

$$\rho \left(\frac{\partial v}{\partial t} + u \frac{\partial v}{\partial x} + v \frac{\partial v}{\partial y} \right) = -\frac{\partial p}{\partial y} + \mu \left(\frac{\partial^2 v}{\partial x^2} + \frac{\partial^2 v}{\partial y^2} \right) - \frac{\mu}{K} v - \frac{\sigma^* B_0^2}{1+m^2} (v + mu) + \rho g \beta (T - T_c) \quad (3)$$

$$\frac{\partial T}{\partial t} + u \frac{\partial T}{\partial x} + v \frac{\partial T}{\partial y} = \alpha \left(\frac{\partial^2 T}{\partial x^2} + \frac{\partial^2 T}{\partial y^2} \right) - \frac{1}{\rho c_p} \left(\frac{\partial q_{rx}}{\partial x} + \frac{\partial q_{ry}}{\partial y} \right) \quad (4)$$

The physical boundary conditions are prescribed as follows:

On all four boundaries (walls): $u = v = 0$

On the top and base walls: $\frac{\partial T}{\partial x} = 0$

On the left wall: $T = T_H$,

On right wall: $T = T_L$ (5)

The magnetic viscous fluid obeys the Newtonian law of viscosity and is optically thick [14].

Therefore, radiative flux is modelled via the Rosseland diffusion approximation [24]:

$$q_{rx} = -\frac{4\sigma}{3\beta} \frac{\partial T^4}{\partial x}, \quad q_{ry} = -\frac{4\sigma}{3\beta} \frac{\partial T^4}{\partial y} \quad (6)$$

By the help of Taylor series, the quartic term T^4 may be expanded in terms of the right cold wall temperature, T_c . Ignoring higher order terms, this leads to the expression [14]:

$$T^4 \approx 4TT_c^3 - 3T_c^4 \quad (7)$$

By the help of Eqn. (7), the radiative heat flux components are reduced to:

$$q_{rx} = -\frac{4\sigma T_c^3}{3\beta} \frac{\partial T}{\partial x}, \quad q_{ry} = -\frac{4\sigma T_c^3}{3\beta} \frac{\partial T}{\partial y} \quad (8)$$

The stream function and vorticity are defined as follows:

$$u = \frac{\partial \psi}{\partial y}, \quad v = -\frac{\partial \psi}{\partial x}, \quad \omega = \frac{\partial v}{\partial x} - \frac{\partial u}{\partial y} \quad (9)$$

Next, introducing the following non-dimensional variables:

$$\tau = \frac{t\alpha}{L^2}, \quad (X, Y) = \frac{(x, y)}{L}, \quad U = \frac{uL}{\alpha}, \quad V = \frac{vL}{\alpha}, \quad P = \frac{pL^2}{\rho\alpha^2}, \quad \theta = \frac{T - T_H}{T_H - T_L}, \quad \Psi = \frac{\psi}{\alpha}, \quad \Omega = \frac{\omega L^2}{\alpha} \quad (10)$$

Implementing the parameters from Eqn. (10), the dimensionless equations now assume the form:

$$\frac{\partial^2 \Psi}{\partial X^2} + \frac{\partial^2 \Psi}{\partial Y^2} = -\Omega \quad (11)$$

$$\frac{\partial \Omega}{\partial \tau} + U \frac{\partial \Omega}{\partial X} + V \frac{\partial \Omega}{\partial Y} = \mathbf{Pr} \left(\frac{\partial^2 \Omega}{\partial X^2} + \frac{\partial^2 \Omega}{\partial Y^2} \right) - \frac{\mathbf{Pr}}{Da} \Omega - \frac{Ha^2 \mathbf{Pr}}{1+m^2} \Omega + \mathbf{RaPr} \frac{\partial \theta}{\partial X} \quad (12)$$

$$\frac{\partial \theta}{\partial \tau} + U \frac{\partial \theta}{\partial X} + V \frac{\partial \theta}{\partial Y} = \left(1 + \frac{4}{3} \mathbf{Rd} \right) \left(\frac{\partial^2 \theta}{\partial X^2} + \frac{\partial^2 \theta}{\partial Y^2} \right) \quad (13)$$

The corresponding dimensionless boundary conditions emerge as:

On all four walls: $U = V = 0$

On top and base walls: $\frac{\partial \theta}{\partial X} = 0$

On left wall: $\theta = 1$ and on the right wall: $\theta = 0$ (14)

In eqns. (12) and (13), $Ra = \frac{\rho g \beta L^3 (T_h - T_c)}{\mu \alpha}$ designates the Rayleigh number, $Pr = \frac{\mu}{\rho \alpha}$ is the

Prandtl number, $Da = K/L^2$ is the Darcy parameter (dimensionless porous medium

permeability), $Ha = LB_0 \sqrt{\frac{\sigma}{\mu}}$ is the Hartmann (magnetic) number i.e. ratio of Lorentz

magnetic body force and viscous hydrodynamic force, and $Rd = -\frac{4\sigma T^3}{k\beta}$ is the thermal

radiation parameter.

The local and average (mean) *Nusselt numbers i. e. wall heat transfer rates* are defined respectively as follows (where Rd is the radiative parameter):

$$Nu = -\left(1 + \frac{4Rd}{3}\right) \left(\frac{\partial\theta}{\partial X}\right)_{X=0} \quad \text{and} \quad Nu_M = -\int_0^1 \left(\frac{\partial\theta}{\partial X}\right) dY \quad (15)$$

3. COMPUTATIONAL SOLUTION

The partial differential equations along with the momentum and thermal boundary conditions (eqn. (11) – eqn. (14)) are solved with a pressure elimination technique and finite difference method i.e., vorticity stream function approach. This numerical approach adopts a collocated grid system with a uniform spacing grid arrangement. The vorticity-stream function approach is a very efficient technique and eliminates the pressure gradient. The explicit time integration scheme can be used to solve the unsteady vorticity transport and thermal equation. However, in all computations we consider only the *steady-state* case i. e. time is neglected. The flow field visualization function i.e. the stream function is solved by the successive over relaxation (SOR) iterative method. The present model, in the form of an in-house CFD code, has been validated successfully against the work of de Vahl Davis [26] and Wan *et al.* [27]. **Table. 1** and **Table. 2** provide good correlation of the present numerical solutions for local Nusselt number for different Rayleigh numbers, against the benchmark studies of de Vahl Davis [26] and Wan *et al.* [27]. The present numerical solutions are in very good agreement with de Vahl Davis [26] and Wan *et al.* [27]. Therefore, confidence in the present in-house code is justifiably high.

4. RESULTS AND DISCUSSION

Figs 2-12 illustrate distributions in the enclosure for streamline contours, temperature contours (isotherms), mid-section velocity profiles and local Nusselt number on the left wall, computed with the present finite difference-based pressure elimination in house MATLAB code. The influence of all key thermophysical and magnetic parameters is addressed in these plots. Data

is prescribed based on electrically conducting air ($Pr = 0.71$), intermediate strength magnetic field ($Ha = 1$) and high permeability porous media ($Da = 0.01$), unless otherwise indicated.

Table. 1. Comparison of average Nusselt number along the hot wall.

	Nu	
	Present	de Vahl Davis [26]
$Ra = 10^4$	2.2526	2.242
$Ra = 10^5$	4.5907	4.523
$Ra = 10^6$	8.9905	9.035

Table. 2. Comparison of average Nusselt number along the hot wall.

	Nu	
	Present	Wan <i>et al.</i> [27]
$Ra = 10^4$	2.2526	2.254
$Ra = 10^5$	4.5907	4.598
$Ra = 10^6$	8.9905	8.976

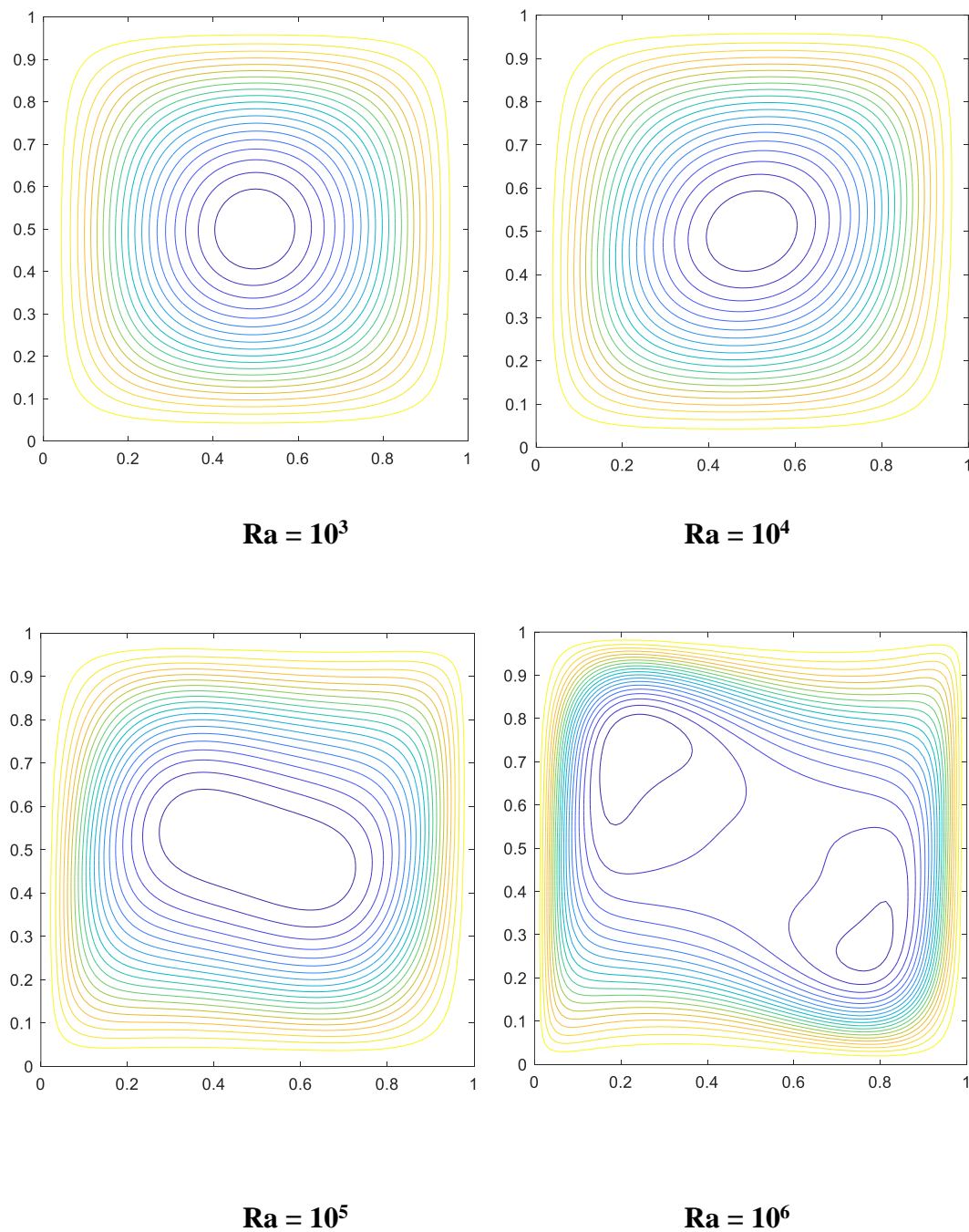


Fig.2. Streamlines variations with the impact of Rayleigh number (Ra) for $Rd = 1$, $Pr = 0.71$,
 $Da = 0.01$, $Ha = 1$, $m = 1$

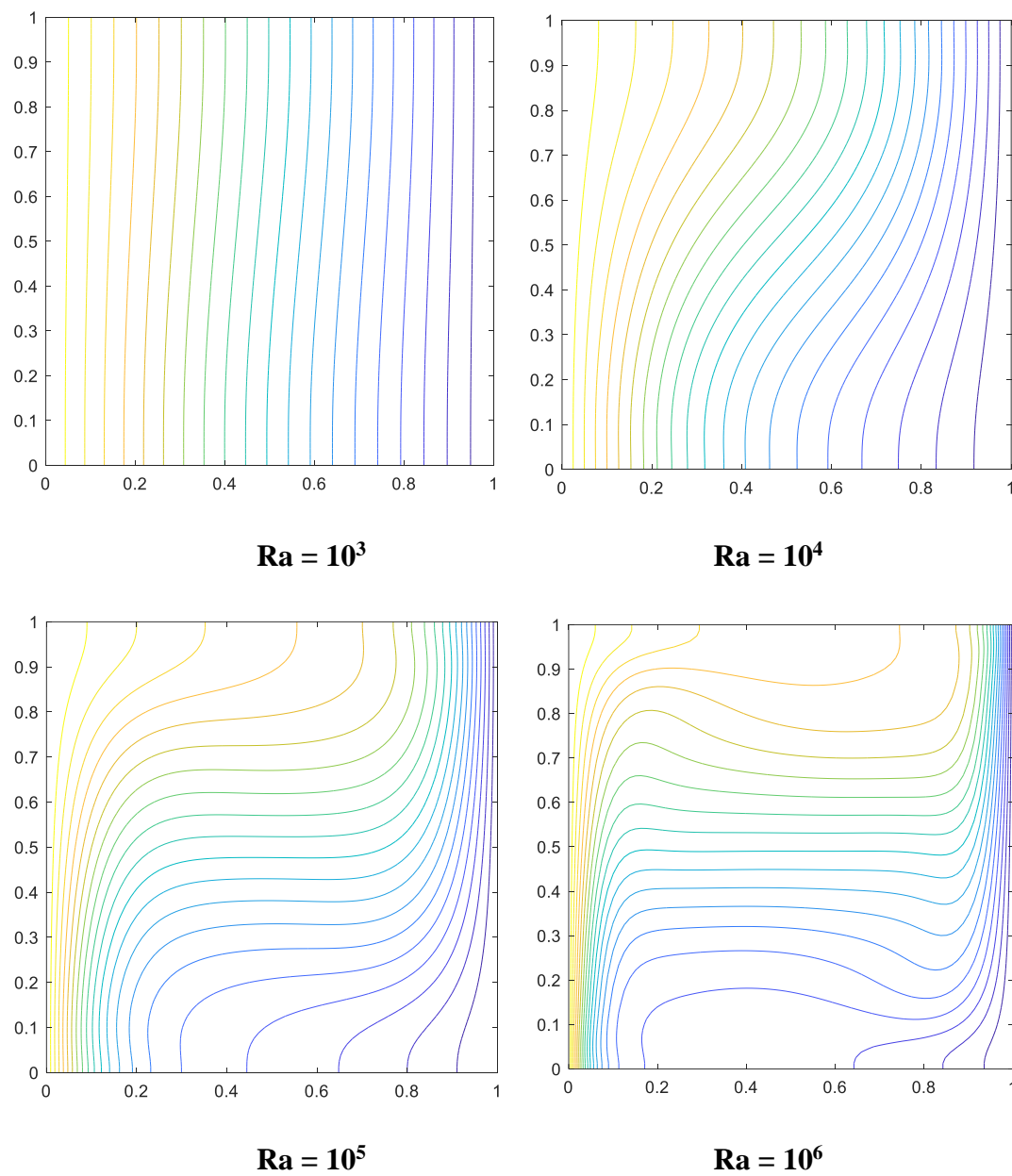


Fig.3. Temperature contours variations with the impact of Rayleigh number (Ra) for $Rd = 1$,
 $Pr = 0.71$, $Da = 0.01$, $Ha = 1$, $m = 1$.

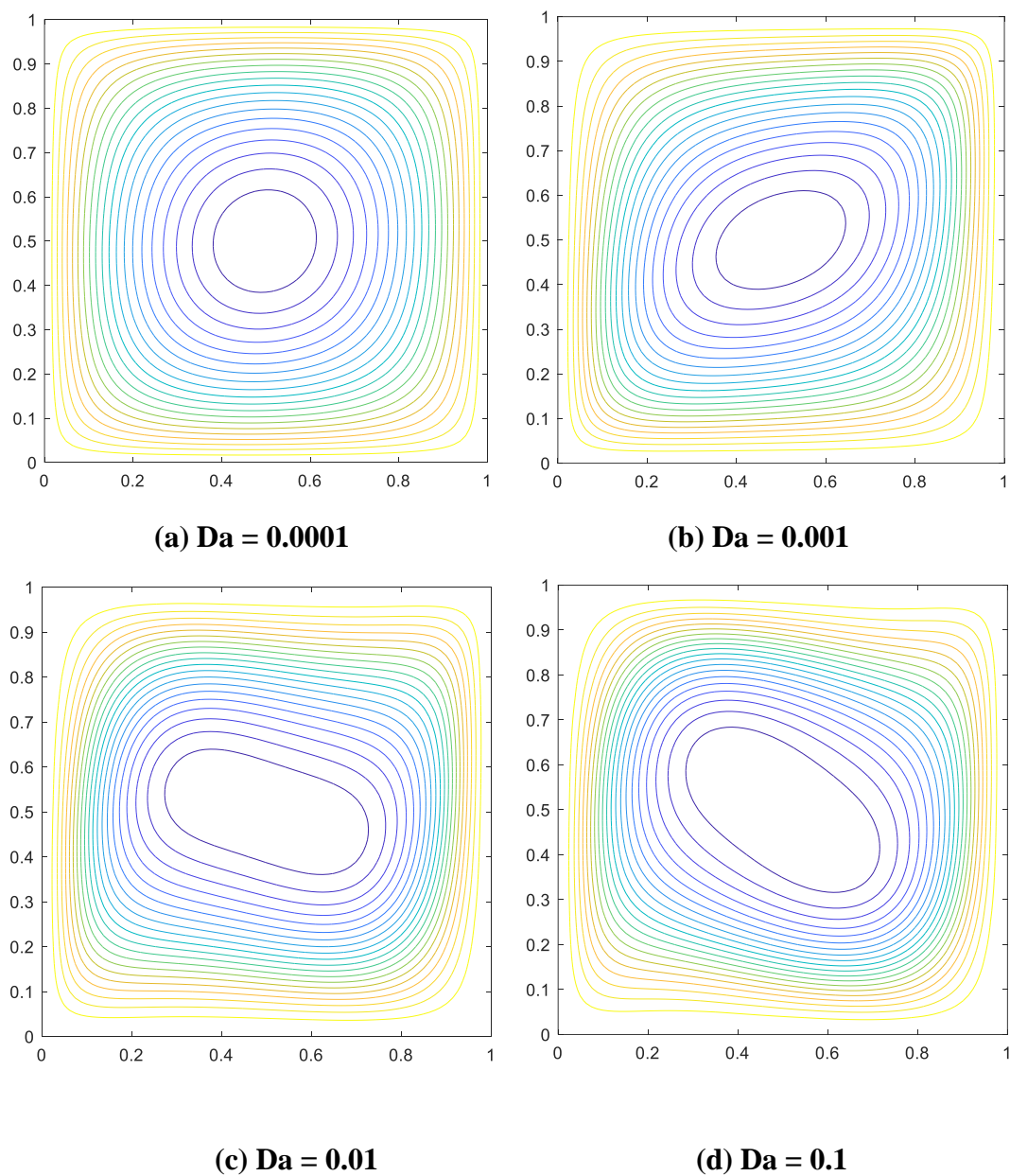


Fig.4. Streamlines variations with the impact of Darcy number (Da) for $Rd = 1$, $Pr = 0.71$,
 $Ra = 10^5$, $Ha = 1$, $m = 1$.

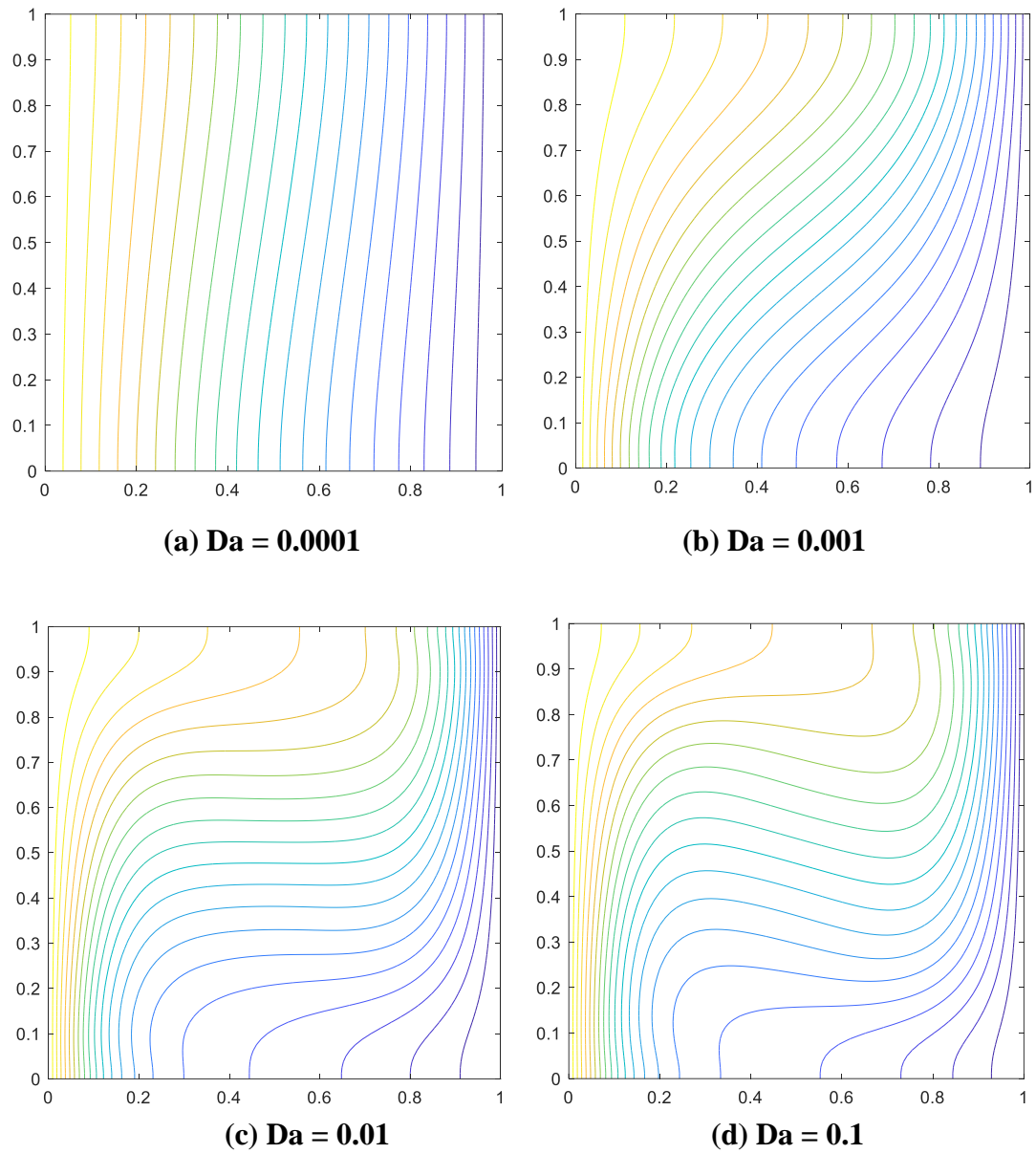


Fig.5. Temperature contours variations with the impact of Darcy number (Da) for $Rd = 1$, $Pr = 0.71$, $Ra = 10^5$, $Ha = 1$, $m = 1$.

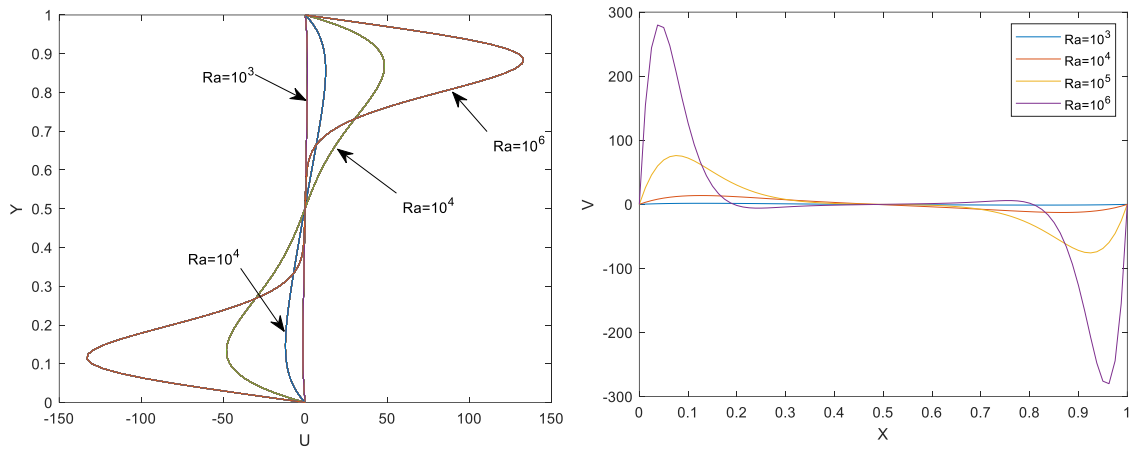


Fig.6. Rayleigh number (Ra) influence on mid-section velocity profiles with $Rd = 1$, $Pr = 0.71$, $Da = 0.01$, $Ha = 1$, $m = 1$.

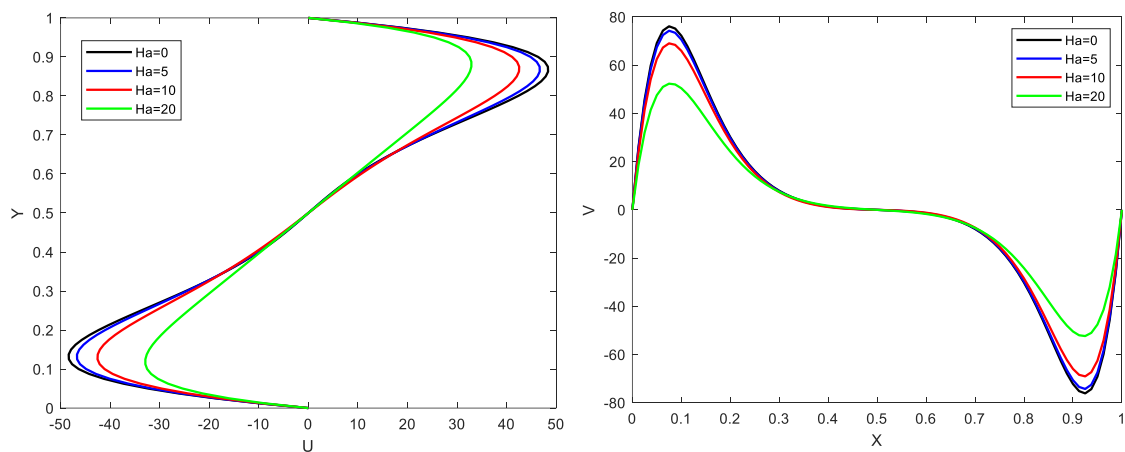


Fig.7. Hartmann number (Ha) influence on mid-section velocity profiles with $Rd = 1$, $Pr = 0.71$, $Da = 0.01$, $Ra = 10^5$, $m = 1$.

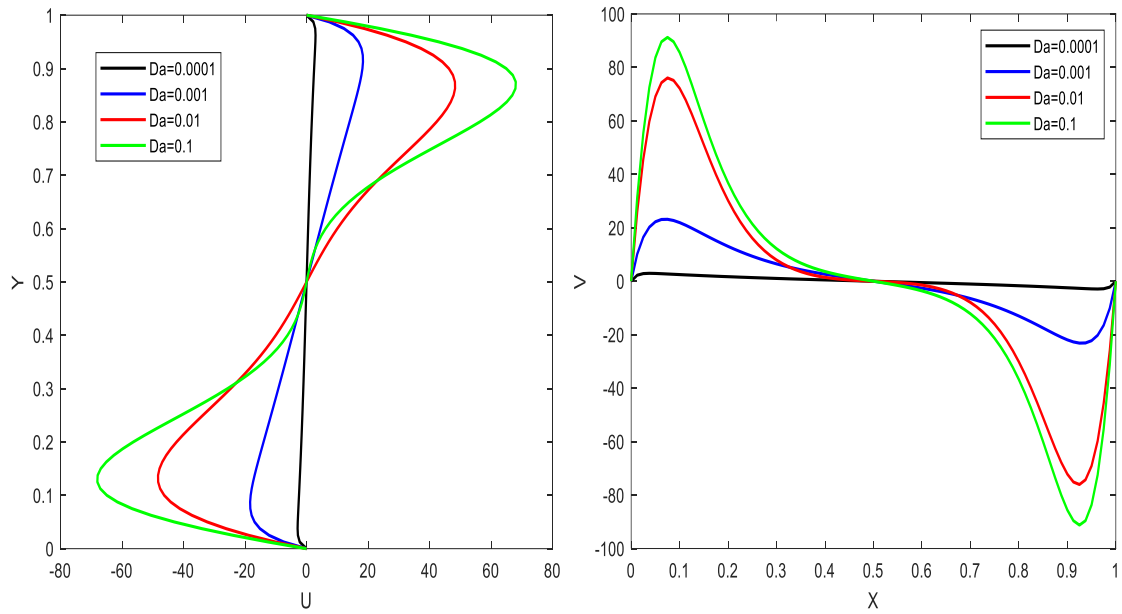


Fig.8. Darcy number (Da) influence on mid-section velocity profiles with $Rd = 1$, $Pr = 0.71$, $Ha = 1$, $Ra = 10^5$, $m = 1$.

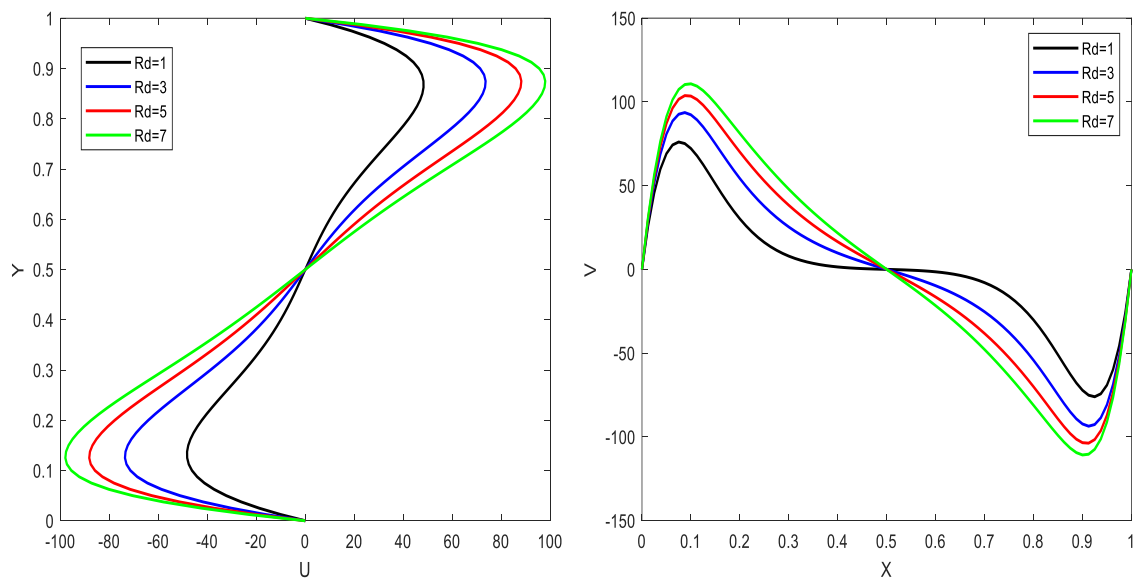


Fig.9. Radiation parameter (Rd) influence on mid-section velocity profiles with $Ha = 1$, $Pr = 0.71$, $Da = 0.01$, $Ra = 10^5$, $m = 12$.

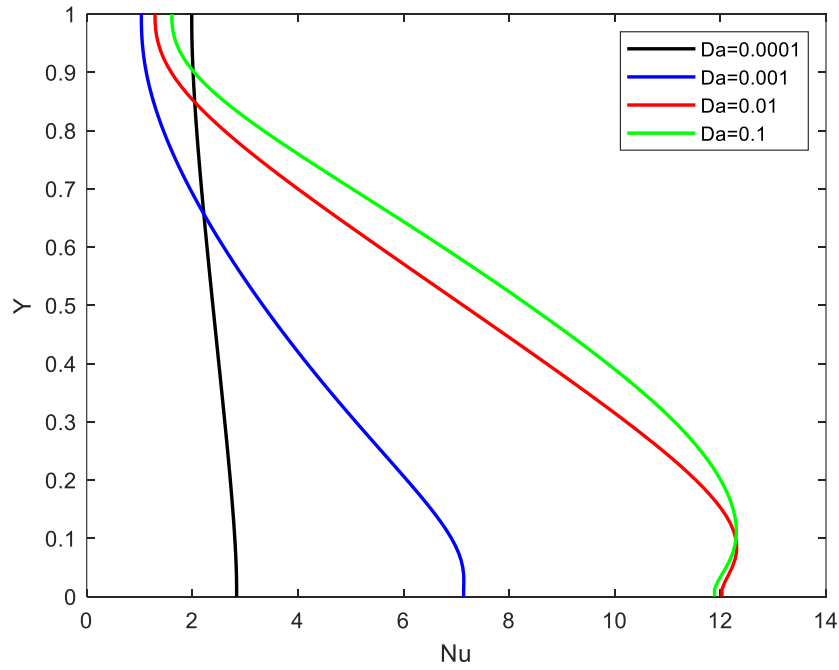


Fig.10. Darcy number (Da) influence on local Nusselt number along the hot wall with $Rd = 1$, $Pr = 0.71$, $Ha = 1$, $Ra = 10^5$, $m = 1$.

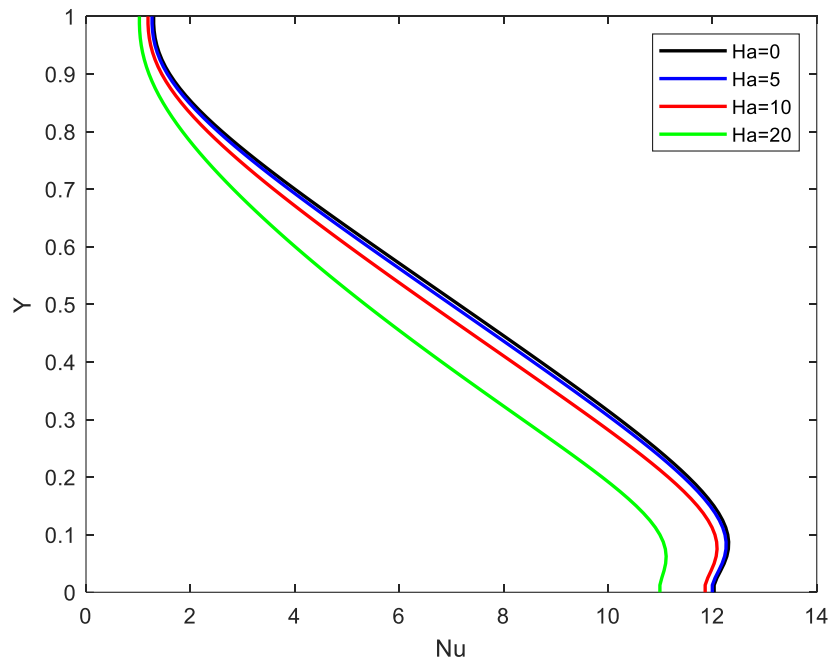


Fig.11. Hartmann number (Ha) influence on local Nusselt number along the hot wall with $Rd = 1$, $Pr = 0.71$, $Da = 0.01$, $Ra = 10^5$, $m = 1$.

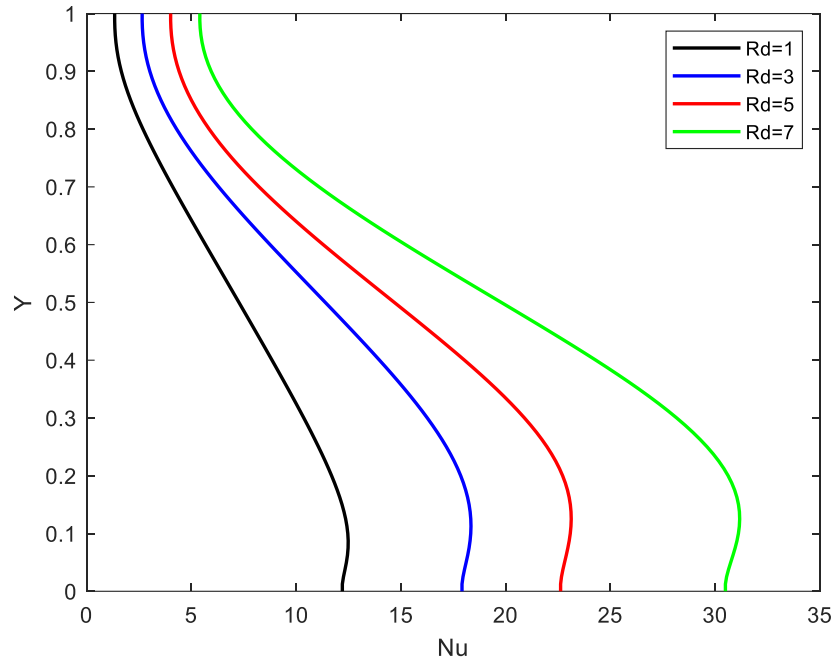


Fig.12. Radiation parameter (Rd) influence on local Nusselt number along the hot wall with $Ha = 1$, $Pr = 0.71$, $Da = 0.01$, $Ra = 10^5$, $m = 1$.

Table. 3. Influence of Hall current parameter (m) and radiative parameter (Rd) on average (mean) Nusselt number with $Ha = 1$, $Pr = 0.71$, $Da = 0.01$, $Ra = 10^5$

	Nu_M			
	$m=1$	$m=5$	$m=10$	$m=20$
Rd=1	7.1451	7.1486	7.1488	7.1489
Rd=3	11.033	11.0406	11.0411	11.0412
Rd=5	14.236	14.2474	14.2481	14.2483
Rd=7	19.1869	19.2023	19.2033	19.2035

Fig.2. visualizes the streamlines distribution with the impact of Rayleigh number (Ra). At low $Ra = 10^3$, there is a single symmetric vortex structure observed in the enclosure. As Rayleigh number increases to $Ra = 10^4$, a distortion is induced in the cell and it is warped diagonally towards the upper right and lower left corners of the enclosure. Asymmetry is therefore produced in the streamline structure. However, with further increment in Rayleigh number to $Ra = 10^5$, i. e. *stronger thermal buoyancy force relative to viscous force*, the *distortion is reversed* and is now much more significant, with a stretching of the cell towards the upper left corner and lower right corner. There is an intensification in the constriction of streamlines at the left hot wall and this is further amplified when the maximum Rayleigh number $Ra = 10^6$ is

considered, for which the single cell bifurcates into a dual structure with a relaxation of streamlines in the central (core) region.

Fig.3 depict the evolution in temperature contours in the enclosure with the impact of Rayleigh number (Ra). At low $Ra = 10^3$, isotherms are almost parallel to the vertical walls i.e. very little distortion is observed. As Ra is increased to 10^4 , and thermal buoyancy is enhanced, isotherms become distorted constricting towards the upper right corner and the lower left corner. Isotherms relax in the upper left corner and lower right corner. Asymmetry is clearly computed in the cavity. The left wall hot zone is progressively pushed further towards the core of the enclosure with higher $Ra = 10^5$ and the upper wall (yellow and green contours) and the base wall and right cold wall are further cooled (blue contours). However subsequent elevation in Rayleigh number to 10^6 , the blue zones are compressed, and the warmer central core expanded to occupy almost all of the upper half space of the enclosure. Thermal buoyancy therefore strongly encourages heat transfer through the enclosure and notably increases temperatures in the upper zone.

Fig.4 visualizes the streamline plots for various Darcy number (Da) in the square enclosure. At low $Da = 0.0001$ (low permeability), there is a symmetric single vortex cell computed in the centre of the enclosure. As permeability increases to $Da = 0.001$, permeability is increased by a factor of 10. There is great decrease in solid matrix fibers offering resistance to the internal circulation and this results in a decrease in Darcian bulk drag which manifests with a distortion in the single vortex cell in a diagonal sense from the lower left corner to the upper right corner. The flow is accelerated and the cell also expands in magnitude. With further increase in permeability to $Da = 0.01$ however this distortion is different- the cell now stretches from the top right corner to the lower left corner and also the topology changes to a more oblong albeit rounded structure. This is further expanded with highest $Da = 0.1$ (very high permeability and very sparsely packed porous medium) and the cell is also slightly rotated anti-clockwise and also becomes sharper at the periphery. Streamlines are strongly compressed at the walls but relaxed around the vortex cell, indicating that permeability (via Darcy number) significantly influences the internal circulation in the enclosure.

Fig.5. displays the contour plots for temperature (isotherms) with the impact of Darcy number (Da). Generally, the streamlines are vertical for low Darcy number owing to the deceleration in the internal flow at low permeability ($Da = 0.0001$). With greater permeability the streamlines ($Da = 0.001$) are distorted and become constricted towards the upper right corner and lower right corner, resulting in asymmetric distributions. Streamlines relax at the upper left and lower right corners. The hot zone originally constrained in the vicinity of the left wall (hot

wall) i.e. yellow/green contours progressively push laterally and occupy the upper zone near the top wall as Da increases to 0.01. This effect is further developed for maximum $Da = 0.1$ and the cold blue zones are constrained closer to right cold wall and lower base wall vicinity. Strong asymmetry is observed in isotherms. Thermal conduction at the periphery of the enclosure is suppressed with greater Darcy number owing to the progressive reduction in solid matrix fibers of the porous medium. However, in the central (core) zone, thermal diffusion is elevated and this results in the expansion of the hot zone increasingly in the central region of the enclosure. Considerable modification in temperature distribution in the enclosure is therefore achieved with greater permeability of the porous medium which is advantageous for fuel cell and materials fabrication designs.

Fig.6. illustrates the effect of Rayleigh number (Ra) on mid-section X-direction and Y-direction velocity profiles (U, V). This provides a perspective of momentum characteristics in the enclosure. Ra features in the assistive body force term $RaPr\frac{\partial\theta}{\partial X}$ in the momentum Eqn. (12). Asymmetry is clearly present at all Rayleigh numbers. However, it is amplified with increasing Rayleigh number. In other words, velocity is greater (higher positive values) towards the upper horizontal wall with greater Rayleigh number, whereas it is progressively reduced (greater negative values) near the base wall with greater Rayleigh number. The weakest asymmetry corresponds to the lowest Rayleigh number. Clearly the implication is acceleration in the upper half space and deceleration in the lower half space of the enclosure which explains the asymmetry computed earlier in the streamline plots. A significant re-distribution in momentum accompanies increasing thermal buoyancy effect relative to viscous effect (increasing Rayleigh number) which can be exploited in fuel cell operations and also manipulation of the velocity field in materials processing applications. However, the secondary velocity, V , demonstrates a very different response. With increment in Rayleigh number, at the left half space of the enclosure there is an acceleration in secondary flow ($0 < X < 0.5$) whereas there is a deceleration in the secondary flow in the right half space ($0.5 < X < 1$). Very little modification is computed at low Rayleigh number (weak thermal buoyancy effect).

Fig.7. visualizes the influence of Hartmann number (Ha) on mid-section X-direction and Y-direction velocity profiles (U, V). $Ha = LB_0\sqrt{\frac{\sigma}{\mu}}$ and appears in the Lorentzian damping term (modified with Hall parameter, m). This term is linear (Eqn. 12) i. e. $\{-Ha^2Pr/(1+m^2)\}\Omega$ in terms of vorticity formulation in the momentum equation. Clearly it is a negative body force which will result in a destruction of momentum (deceleration) in the upper half space of the

enclosure. This deceleration is compensated for with an acceleration in the upper half space although U-velocities are still negative for $0.5 < Y < 1$ whereas they are generally positive for $0.5 < Y < 1.0$. Hartmann number increasing implies greater magnetic Lorentz force which significantly damps the flow in the enclosure. For the case $Ha = 0$, magnetic force vanishes, and the air is electrically non-conducting. The Y-direction velocity is also strongly reduced with increment in Ha for $0 < X < 0.5$ whereas it is accelerated (values become less negative) for $0.5 < X < 1$, again due to momentum re-distribution in the closed cavity system. Strong asymmetry is computed again for both velocity components and this corresponds to the asymmetric streamline plots discussed earlier. The excellent damping nature of external magnetic field is therefore clearly demonstrated and may be exploited, for example, to regulate internal flow structures in hybrid fuel cells designs.

Fig.8. visualizes the influence of Darcy number (Da) on mid-section X-direction and Y-direction velocity profiles (U, V). $Da = K/L^2$ and appears in the Darcian body force term which is also linear in Eqn. (12) i. e. $-(Pr/Da)\Omega$ in terms of the vorticity formulation in the momentum equation. Increasing Darcy number strongly accelerates the U velocity for $0.5 < Y < 1$, whereas it decelerates the U velocity for $0 < Y < 0.5$, again due to momentum re-distribution in the enclosure. V velocity is strongly enhanced for $0 < X < 0.5$ whereas it is reduced for $0.5 < X < 1$. Therefore, while permeability increasing reduces the Darcian drag force, it only induces acceleration in certain zones of the enclosure. This again explains the asymmetry in streamlines computed earlier since there is no consistent acceleration in the percolating flow throughout the enclosure porous regime with merely an increment in permeability (Darcy number). Local zones of deceleration are also produced. Nevertheless, the presence of a porous medium can be utilized to effectively modify the internal flow structures in for example fuel cells and materials synthesis operation.

Fig.9. shows the effects of radiation parameter (Rd) on mid-section X-direction and Y-direction velocity profiles (U, V). Rd features in appears in the augmented thermal conduction terms,

$$\left(1 + \frac{4}{3} \mathbf{Rd}\right) \left(\frac{\partial^2 \theta}{\partial X^2} + \frac{\partial^2 \theta}{\partial Y^2}\right), \text{ in the energy conservation eqn. (13). } Rd = -\frac{4\sigma T_c^3}{k\beta}$$

relative contribution of thermal radiation to thermal conduction heat transfer. For $Rd = 1$ both modes contribute equally. When $Rd > 1$ thermal radiative flux dominates and vice versa for $Rd < 1$. Increasing Rd energizes the flow in the enclosure and leads to acceleration in the U velocity in the region $0.5 < Y < 1$ (upper half space) whereas it decelerates the primary flow (U velocity) in the region $0 < Y < 0.5$, in the lower half space. Similarly, the V velocity (secondary flow) is

strongly accelerated in the left half space of the enclosure ($0 < X < 0.5$) whereas it is decelerated markedly in the right half space ($0.5 < X < 1.0$). For both primary and secondary flows, the minimum velocity magnitudes correspond to the weakest case of thermal radiation i. e. $Rd = 1$ (black line). Clearly thermal radiative flux has a substantial influence on velocity fields in the enclosure and neglect of this important mode of heat transfer leads to erroneous computations in high temperature enclosure MHD flow simulations.

Fig.10. illustrates the effect of Darcy number (Da) on local Nusselt number along the hot wall (left vertical wall). With increasing Darcy number and correspondingly reducing Darcian drag force (higher permeability of the porous medium), there is a strong elevation in local Nusselt number. Heat transfer rate to the hot wall is therefore elevated with greater Darcy number. This implies that more heat is diffused away from the internal regime to the hot wall which also explains the decrease in temperatures (isotherm magnitudes) computed in earlier plots with higher Darcy number. The porous medium therefore can be manipulated to achieve desired heat transfer to the boundaries which is very important in cooling fuel cells systems and preventing over-heating. Porous media can also be utilized to regulate heat flux to the boundaries of materials fabrication systems and provide an inexpensive and dependable mechanism for thermal management.

Fig.11. displays the effect of Hartmann number (Ha) on local Nusselt number along the hot wall (left vertical wall). With increasing Hartmann number there is a strong depletion in local Nusselt number. Heat transfer rate to the hot wall is therefore reduced with greater magnetic field intensity. The Lorentz body force is greater for higher Ha values. Greater kinetic energy has to be expended to drag the internal percolating fluid against the action of a stronger magnetic field. This supplementary energy is dissipated as heat leading to elevation in temperatures inside the body of the enclosure. This results in a greater transfer of heat to the fluid regime and a corresponding reduction in heat transferred to the boundaries. Heat transfer to the left vertical hot wall is therefore suppressed and Nusselt number is reduced. Thermal convection relative to thermal conduction at the hot wall is also depleted (Nusselt number also quantifies the ratio of thermal convection to thermal conduction). Stronger external magnetic field therefore successfully regulates heat flux to the hot wall which is advantageous in fuel cell thermal control.

Fig.11. displays the effect of radiation parameter (Rd) on local Nusselt number along the hot wall (left vertical wall). With increasing radiative flux intensity there is an elevation in rd . This generates higher transport of heat to the hot wall which results in considerable elevation in local Nusselt number. Thermal convection relative to thermal conduction at the hot wall are

therefore increased. The effect is opposite to that of increasing magnetic field. Designers therefore may judiciously select the magnitude of radiative flux to limit the heat transfer to the enclosure boundary and furthermore may exploit magnetic field to achieve this thermal control. Higher local Nusselt numbers are also localized towards the lower half space and much smaller towards the upper half space of the enclosure.

Finally, **Table. 3** shows the influence of Hall current parameter (m) and also radiative parameter (Rd) on average (mean) Nusselt number. Increasing Hall effect clearly strongly elevates the mean Nusselt number, at any value of radiative parameter. The Hall effect influences the secondary flow field and decreases temperatures in the enclosure. This elevates the heat transferred to the boundary and leads to elevation in the mean Nusselt number. As noted earlier, there is a strong enhancement in heat transferred to the boundary (hot wall) with greater radiative flux (Rd) which produces substantial increment in average Nusselt numbers computed. Hall parameter has a greater effect at higher radiative parameters and clearly inclusion of the Hall parameter (m) is important in achieving more realistic predictions of magnetohydrodynamic heat transfer in fuel cells.

5. CONCLUSIONS

A new mathematical model has been developed for two-dimensional viscous magnetohydrodynamic radiative-convective flow in a square enclosure containing a Darcian porous medium with Hall currents. The formulated nonlinear boundary value problem comprising the mass, momentum and energy conservation equations with appropriate wall boundary conditions, has been rendered dimensionless via appropriate scaling transformations. The resulting non-dimensional boundary value problem has been solved computationally with a finite-difference vorticity stream function approach executed in MATLAB software. A detailed parametric investigation of the impact of Rayleigh number (thermal buoyancy parameter), Hartman number (magnetic body force parameter), Darcy number (permeability parameter), Hall parameter and radiation parameter on the streamline, temperature contours, local Nusselt number along the hot wall and mid-section velocity profiles has been conducted. The present simulations have shown that:

- Rayleigh number can be a control key parameter on heat and flow in enclosures. In addition, the heat transfer rate is intensified with increasing of Rayleigh number.

Multiple fluid circulations and higher heat transfer rates are noticed at greater values of Rayleigh number Ra .

- Increasing Hall parameter effect strongly influences the secondary flow field and decreases temperatures in the enclosure, with a corresponding enhancement in mean Nusselt number at the left hot wall of the enclosure.
- Increasing Hartmann number strongly reduces heat transfer to the left vertical hot wall i.e., decreases local Nusselt number values.
- With increasing Darcy number (i.e., greater permeability of the porous medium and progressively lower Darcian drag force) there is a strong elevation in local Nusselt number at the left hot wall.
- With increasing radiative parameter, acceleration in the U velocity is induced in the region $0.5 < Y < 1$ (upper half space) whereas deceleration in the primary flow (U velocity) in the region $0 < Y < 0.5$, in the lower half space. Similarly, the V velocity (secondary flow) is strongly accelerated in the left half space of the enclosure ($0 < X < 0.5$) whereas it is decelerated markedly in the right half space ($0.5 < X < 1.0$).
- Streamlines are strongly compressed at the walls but relaxed around the vortex cell, indicating that permeability (via Darcy number) significantly influences the internal circulation in the enclosure.
- With increasing Rayleigh number, strong asymmetry is clearly computed in the cavity vortex flow structure. Thermal buoyancy therefore strongly encourages heat transfer through the enclosure and significantly enhances temperatures in the upper zone.

The present simulations have provided some interesting insights into magnetohydrodynamic viscous convection flows in enclosures with thermal radiative and Hall current effects. The finite difference method deployed has demonstrated excellent accuracy. However magnetic induction has been neglected. Future studies may consider magnetic induction [28] and furthermore nanofluids [29] which are becoming increasingly popular in modern hybrid fuel cell designs and also manufacturing processes exploiting nanotechnology.

REFERENCES

- [1] Rosensweig, R. E., and J. Popplewell. "Electromagnetic Forces and Applications." *Int. J. Appl. Electromag. Mater* 2 (1992): 83-86.
- [2] Zhang, Sam, and Dongliang Zhao, eds. *Advances in magnetic materials: processing, properties, and performance*. CRC press, 2017.
- [3] Gebhart, B., Y. Jaluria, R. L. Mahajan, and B. Sammakia. "Buoyancy-induced flows and transport hemisphere." *New York* (1988): 53.
- [4] Hjellming, L. N., and J. S. Walker. "Melt motion in a Czochralski crystal puller with an axial magnetic field: isothermal motion." *Journal of Fluid Mechanics* 164 (1986): 237-273.
- [5] Takagi, Youhei, Yasunori Okano, and Sadik Dost. "A numerical simulation study on the effects of crucible rotation and magnetic fields in growth of SiGe by the traveling heater method." *Journal of heat transfer* 134, no. 1 (2012).
- [6] Biswas, Nirmalendu, and Nirmal K. Manna. "Magneto-hydrodynamic Marangoni flow in bottom-heated lid-driven cavity." *Journal of Molecular Liquids* 251 (2018): 249-266.
- [7] Hussain, S., K. Mehmood, and M. Sagheer. "MHD mixed convection and entropy generation of water–alumina nanofluid flow in a double lid driven cavity with discrete heating." *Journal of Magnetism and Magnetic Materials* 419 (2016): 140-155.
- [8] Mohan, C. G., and A. Satheesh. "The numerical simulation of double-diffusive mixed convection flow in a lid-driven porous cavity with magnetohydrodynamic effect." *Arabian Journal for Science and Engineering* 41, no. 5 (2016): 1867-1882.
- [9] Mondal, Milan K., Nirmalendu Biswas, and Nirmal K. Manna. "MHD convection in a partially driven cavity with corner heating." *SN Applied Sciences* 1, no. 12 (2019): 1-19.
- [10] Haq, Rizwan Ul, Feroz Ahmed Soomro, Toufik Mekkaoui, and Qasem M. Al-Mdallal. "MHD natural convection flow enclosure in a corrugated cavity filled with a porous medium." *International Journal of Heat and Mass Transfer* 121 (2018): 1168-1178.
- [11] Kefayati, GH R. "FDLBM simulation of magnetic field effect on mixed convection in a two sided lid-driven cavity filled with non-Newtonian nanofluid." *Powder technology* 280 (2015): 135-153.
- [12] Daun, K. J., S. B. Beale, F. Liu, and G. J. Smallwood. "Radiation heat transfer in planar SOFC electrolytes." *Journal of Power Sources* 157, no. 1 (2006): 302-310.
- [13] Mansour, R. B., and R. Viskanta. "Radiative and convective heat transfer for materials processing." In *Proceedings of the First Conference on Transport Phenomena in Processing, (SI Guceri, Editor), Technomic Publishing Co., Lancaster, PA, USA*, pp. 693-713. 1992.
- [14] Hottel, Hoyt C., and Adel F. Safirim. "Radiative transfer." McGraw-Hill, New York (1967).

- [15] Muiznieks, A., A. Krauze, and B. Nacke. "Convective phenomena in large melts including magnetic fields." *Journal of crystal growth* 303, no. 1 (2007): 211-220.
- [16] Saidin, M. K. B., G. J. Russell, A. W. Brinkman, and J. Woods. "Hall mobility and conductivity in $Zn_xCd_{1-x}S$ mixed crystals." *Journal of crystal growth* 101, no. 1-4 (1990): 844-849.
- [17] Brunner, MJt. "The Effects of Hall and Ion Slip on the Electrical Conductivity of Partially Ionized Gases for Magnetohydrodynamic Re-Entry Vehicle Application." (1962): 177-184.
- [18] Roschke, E. J. "Experimental investigation of heat transfer from partially ionized argon with an applied transverse magnetic field." (1972): 174-180.
- [19] Wang, Yixiao, Ji-Gou Liu, Jing Zhao, and Yongcai Yang. "Split core closed loop Hall effect current sensors and applications." In *PCIM EUROPE International Exhibition and Conference for Power Electronics, Intelligent Motion, Power Quality, Nuremberg, Germany*, pp. 1633-1638. 2012.
- [20] Anwar Beg, O., M. Ferdows, M. Enamul Karim, M. Maruf Hasan, Tasveer A. Bég, M. D. Shamshuddin, and A. Kadir. "Computation of non-isothermal thermo-convective micropolar fluid dynamics in a Hall MHD generator system with non-linear distending wall." *International Journal of Applied and Computational Mathematics* 6, no. 2 (2020): 1-44.
- [21] Zhang, Jing-Kui, Ben-Wen Li, and Yuan-Yuan Chen. "The joule heating effects on natural convection of participating magnetohydrodynamics under different levels of thermal radiation in a cavity." *Journal of Heat Transfer* 137, no. 5 (2015).
- [22] Zhang, Jing-Kui, Ben-Wen Li, and Yuan-Yuan Chen. "Hall effects on natural convection of participating MHD with thermal radiation in a cavity." *International Journal of Heat and Mass Transfer* 66 (2013): 838-843.
- [23] Bég, O. Anwar, K. Venkatadri, V. Ramachandra Prasad, T. A. Beg, A. Kadir, and Henry J. Leonard. "Numerical simulation of hydromagnetic Marangoni convection flow in a Darcian porous semiconductor melt enclosure with buoyancy and heat generation effects." *Materials Science and Engineering: B* 261 (2020): 114722.
- [24] O. Anwar Bég, K. Venkatadri, V.R. Prasad, Tasveer A. Bég, Henry J. Leonard, MAC computation of magnetohydrodynamic convection flow in a non-Darcian porous enclosure saturated with electrically conducting Helium, *Proc. IMechE-Part C – J. Mechanical Engineering Science* (2021). 21 pages. DOI: 10.1177/09544062211003624
- [25] Venkatadri, K., O. Anwar Bég, and V. Ramachandra Prasad. "Numerical simulation of thermal management during natural convection in a porous triangular cavity containing air and hot obstacles." *The European Physical Journal Plus* 136, no. 8 (2021): 1-18.

- [26] De Vahl Davis, G., Natural convection of air in a square cavity: a benchmark numerical solution. *International Journal for Numerical Methods in Fluids*, 3 (1983) 249-264.
- [27] D. C. Wan, B. S. V. Patnaik, and G. W. Wei, A new benchmark quality solution for the buoyancy-driven cavity by discrete singular convolution, *Numerical Heat Transfer, Part B*, 40 (2001) 199- 228.
- [28] Lee, Myoungwoo, and Youn-Jea Kim. "Thermomagnetic convection of ferrofluid in an enclosure channel with an internal magnetic field." *Micromachines* 10, no. 9 (2019): 553.
- [29] Kuharat, Sireetorn, O. Anwar Bég, Ali Kadir, and B. Vasu. "Computation of metallic nanofluid natural convection in a two-dimensional solar enclosure with radiative heat transfer, aspect ratio and volume fraction effects." *Arabian Journal for Science and Engineering* 45, no. 11 (2020): 9075-9093.
- [30] Sankar, M., N. Keerthi Reddy, and Younghae Do. "Conjugate buoyant convective transport of nanofluids in an enclosed annular geometry." *Scientific Reports* 11, no. 1 (2021): 1-22.
- [31] Sankar, M., M. Venkatachalappa, and I. S. Shivakumara. "Effect of magnetic field on natural convection in a vertical cylindrical annulus." *International Journal of Engineering Science* 44, no. 20 (2006): 1556-1570.
- [32] Venkatachalappa, M., Younghae Do, and M. Sankar. "Effect of magnetic field on the heat and mass transfer in a vertical annulus." *International Journal of Engineering Science* 49, no. 3 (2011): 262-278.
- [33] Sivasankaran, S., Younghae Do, and M. Sankar. "Effect of discrete heating on natural convection in a rectangular porous enclosure." *Transport in porous media* 86, no. 1 (2011): 261-281.
- [34] Makinde, Oluwole Daniel, and M. Sankar. "Numerical investigation of developing natural convection in vertical double-passage porous annuli." In *Defect and Diffusion Forum*, vol. 387, pp. 442-460. Trans Tech Publications Ltd, 2018.
- [35] Girish, N., M. Sankar, and Keerthi Reddy. "Analysis of fully developed mixed convection in open-ended annuli with viscous dissipation." *Journal of Thermal Analysis and Calorimetry* 143, no. 1 (2021): 503-521.